INSTITUTE OF PHYSICS PUBLISHING and INTERNATIONAL ATOMIC ENERGY AGENCY NUCLEAR FUSION

Nucl. Fusion **44** (2004) 799–810 PII: S0029-5515(04)80969-4

Improved confinement events triggered by emissive electrode biasing on the tokamak ISTTOK

C. Silva, I. Nedzelskiy, H. Figueiredo, R.M.O. Galvão[a], J.A.C. Cabral and C.A.F. Varandas

Associação Euratom/IST, Centro de Fusão Nuclear, Instituto Superior Técnico, 1049-001 Lisbon, Portugal

Received 17 February 2004, accepted for publication 14 May 2004
Published 8 June 2004
Online at stacks.iop.org/NF/44/799
doi:10.1088/0029-5515/44/7/012

Abstract
Edge polarization experiments were carried out on ISTTOK using an emissive electrode. The dependence of the bias current on the radial electric field, measured by a radial array of Langmuir probes, is in qualitative agreement with the expression derived by Stringer for the transitional region between plateau and collisional transport regimes (Stringer T.E. 1993 *Nucl. Fusion* **33** 1249). Improved particle confinement is clearly observed for negative bias associated with a large radial electric field. In some cases, a double-peaked profile of the radial electric field is observed just after biasing, evolving afterwards to a single-peaked profile as confinement improves. These types of profiles may be related to the multiple solutions of the non-linear equation for the radial electric field, recently put forward by Kasuya *et al* (2003 *Nucl. Fusion* **43** 244). Above a certain threshold of the bias current stronger improved confinement events are observed, during short periods, for both bias polarities.

PACS numbers: 5240H, 5255F

1. Introduction

The observation that an improved energy confinement regime could be triggered by electrostatic polarization of the plasma edge in the CCT tokamak [1] led to intense investigation of the plasma response to edge polarization under different conditions. Weynants and Taylor [2] have shown that the transition is related to the non-linear dependence of the radial plasma current on the radial electric field and that this non-linearity is predicted by some of the mechanisms proposed to explain the damping of poloidal rotation in tokamak discharges. The original results obtained in CCT were confirmed and extended by further work carried out in various tokamaks [3–10] and many different theoretical models were developed to explain the experimental findings [11–17]. In particular, Stringer [17] derived an expression for the radial current driven by the radial electric field, which is valid in the transition region between the semi-collisional (plateau) and collisional transport regimes, and showed that a bifurcation in the steady solution for the radial electric field, under appropriate boundary conditions, is expected beyond a critical value of the field, which depends on local plasma conditions. Recently, Kasuya *et al* [18] have shown that the equation for the radial electric field, in the presence of edge electrode biasing, allows for various types of field structures, with multiple peaks, for the same boundary condition. In a subsequent work, they suggested that a double-peaked structure could be driven by edge biasing with two radially displaced electrodes [19].

Electrode biasing experiments have been previously investigated in detail in the tokamak ISTTOK [20]. For positive electrode bias, the plasma potential profile was strongly modified in the region between the electrode and the limiter (values of E_r larger than $10\,\mathrm{kV\,m^{-1}}$ have been measured), leading to improvement in gross particle confinement. However, for negative bias ($-250 < V_{\mathrm{bias}} < 0\,\mathrm{V}$) no significant modification of either the global or the edge plasma parameters were observed due to the low current drawn by the electrode ($\sim$1 A). In order to obtain the larger current necessary to modify confinement at negative applied voltages, two different approaches have been followed in biasing experiments: (i) use of a small limiter, inserted deep inside the main limiter radius and (ii) use of a small emissive electrode made of lanthanum hexaboride (LaB_6). Limiter biasing experiments were the first to be performed and the results showed that, in spite of the strong perturbation of the discharge introduced by the limiter due to its large

[a] Permanent address: Instituto de Física, Universidade de São Paulo, 05315-970, SP, Brazil.

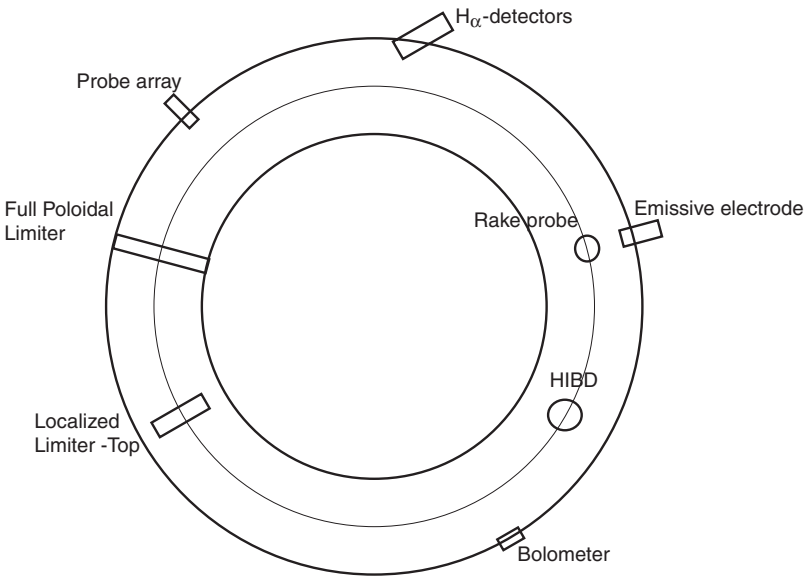

Figure 1. Schematic illustration of ISTTOK (top view) showing the main elements of the experiment.

area, confinement improvement could be obtained for both polarities [21].

Emissive electrode bias (EEB) is also expected to produce large currents in the edge plasma, allowing an effective control of the local plasma potential at negative bias. Although emissive electrodes were used in one of the first biasing experiments in tokamaks [22], its use has been very limited in fusion plasmas. The injection of electrons was used in the Macrotor tokamak to control the sheath potential and consequently reduce the metallic impurities influx. A decade later, electron-emissive injectors (W, LaB_6) were used in the CCT tokamak [1] and a clear transition to the H-mode has been observed. More recently, biasing experiments were carried out in the MST reversed field pinch with electrons emitted from miniature plasma sources at the edge of the plasma column and, once more, a clear improvement in particle confinement was observed [23].

In this work, we report on the results of edge polarization experiments carried out in ISTTOK using an emissive electrode. The main result of these experiments is the discovery of improved confinement events (ICEs), which are characterized by a steady increase of the plasma density associated with a decrease of the H_α radiation. These events are observed for both negative and positive bias, provided that the bias current is larger than a threshold value, $|I_{\rm bias}| \approx 20$ A. As the polarization voltage is increased, the bias current starts to increase linearly with the radial electric field and reaches a saturation value, after which it decreases, in qualitative agreement with the Stringer expression for the radial current density [17]. In some cases, the radial profile of the radial electric field shows a double-peaked structure at the beginning of an ICE, and later relaxes to a single-peaked structure, as the density increases towards its maximum during the event. These structures may be related to the non-linear solutions of the equation for the radial electric field, recently discussed by Kasuya *et al* [18].

The experimental set-up is discussed in the next section. The experimental results for both negative and positive bias are presented in section 3. A brief discussion of the results and the conclusions are given in section 4.

2. Experimental set-up

A schematic illustration of ISTTOK (top view) is presented in figure 1, showing the main elements of the experiment. ISTTOK is a large aspect ratio circular cross-section tokamak ($R = 46$ cm, $a = 7.8$ cm, $B_{\rm T} = 0.5$ T, $\Delta\Phi = 0.22$ V s), which has a fully poloidal graphite limiter at $r = 7.8$ cm and a small stainless steel localized limiter consisting of a section of a poloidal limiter, covering an angular extension of approximately 90°. For the experimental results reported in this paper, the typical values of the ISTTOK discharge parameters were: plasma current $I_{\rm p} \approx$ 5–6 kA, discharge duration $\tau_{\rm d} \approx$ 30–40 ms, central electron density $n_{\rm e}(0) \approx$ (5–10) $\times 10^{18}$ m^{-3}, central electron temperature $T_{\rm e}(0) \approx$ 150–200 eV, particle confinement time $\tau_{\rm p} \sim 0.5$ ms, toroidal beta value $\beta \sim 0.5\%$ and edge safety factor $q(a) \approx 5$.

A radial array of Langmuir probes (rake probe), located in the same toroidal position of the emissive electrode, has been used to study the influence of biasing on the boundary plasma. The rake probe consists of a boron nitride head carrying nine tungsten tips and covering an extension of 27 mm (spatial resolution down to 4 mm). Two of the probes are at the same radial position and used to measure the parallel Mach number. A second array of Langmuir probes, toroidally located at about 120° from the emissive electrode, and consisting of three probes poloidaly separated, has been used mainly to estimate the turbulent particle flux.

A heavy ion beam diagnostic (HIBD) was also available during the experiments. With the HIBD, the radial profiles of the product $n_{\rm e}\sigma_{\rm eff}$ (where $\sigma_{\rm eff}$ is the effective cross-section of the double ionization process) were measured. The time evolution of the central value of the $n_{\rm e}\sigma_{\rm eff}$ profile, measured by the HIBD, is well correlated with that of the line-averaged density, $n_{\rm e}$. Good quality profiles are obtained in the region

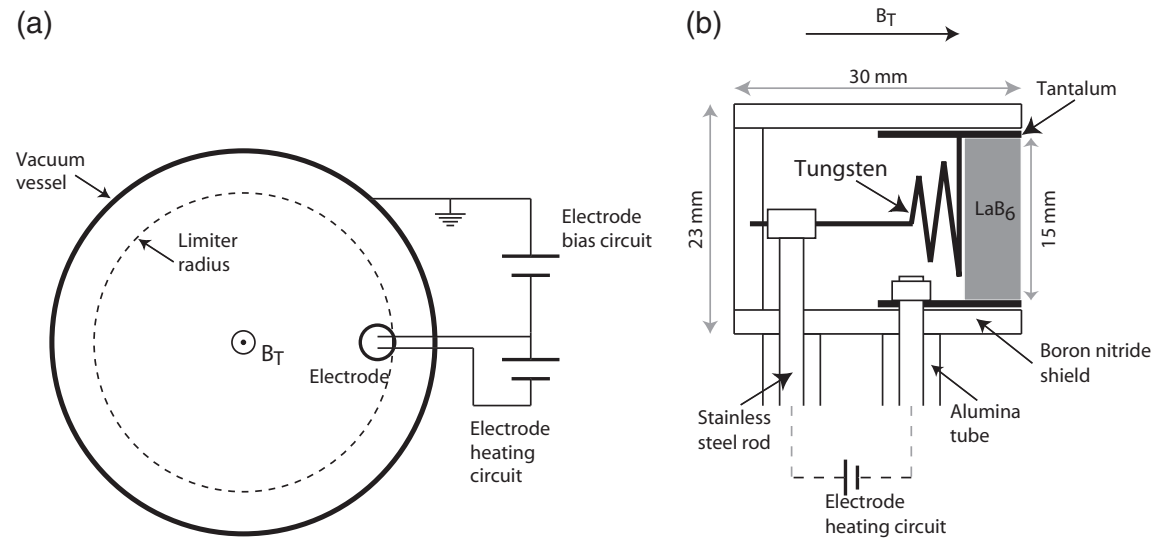

Figure 2. Schematic drawing of the bias and heating circuits (*a*) and the emissive electrode (*b*).

$r < 5$ cm. Outside that region, the signal-to-noise ratio is poor. The Langmuir probes complement, therefore, the HIBD.

A movable emissive electrode has been developed for the biasing experiments in ISTTOK. The bias circuit is presented in figure 2(*a*) and the electrode head is depicted schematically in figure 2(*b*). The emissive electrode consists of a LaB_6 disk with a diameter of 16 mm and covered by a tantalum cylinder, which is protected by a boron nitride cup as the insulating material to be exposed to the plasma. The emissive electrode is aligned with the magnetic field and facing the direction opposite to the plasma current, to avoid possible damage caused by runaway electrons. The bias voltage is applied between the electrode and the vacuum vessel. Up to 30 A of steady state current can be emitted along the magnetic field, returning to the wall by cross-field transport. We find that the emitted current, I_{em}, increases with the emitter temperature in rough agreement with the Richardson–Dushman formula, which is characterized by an approximately zero current up to a threshold electrode temperature ($\approx$1700 K) and then a fast current increase above that value.

3. Discharge behaviour with negative and positive electrode bias

The effect of an emissive electrode, as compared to a non-emissive one, can be qualitatively understood from the basic theoretical model for emissive electrostatic probes [24]. Emissive probes consist of a wire probe heated to emit electrons. As the emission current increases, the emitted electrons reduce the sheath voltage and the floating potential approaches the plasma potential. However, it has been found that the difference between the potential of the emissive and cold probe is less than the value predicted by probe theory and that space charge effects may explain this discrepancy [24]. When a negative probe potential with respect to the plasma potential is imposed, a substantial current is emitted from the probe to the plasma. If the emission current is substantially augmented, space charge effects start to play a role on the probe characteristic, not only changing its floating potential [25], but also giving rise to non-linear potential structures close to it [26]. For positive bias, we expect the probe to behave just as a non-emissive one.

3.1. Negative bias

The result of negative electrode bias for low values of the bias current ($V_{bias} = -100$ V, $|I_{bias}| < 15$ A) can be seen in figure 3. The electrode bias was applied in periodic pulses of 1 ms duration, with the same time interval between pulses, and the electrode is located 12 mm inside the last-closed flux surface (LCFS). In the periods between the applied bias pulses, the electrode bias circuit is open and therefore the applied voltage signal measures the electrode floating potential. As expected, the current driven by the emissive electrode is significantly larger than the ion saturation current for the same electrode, $I_{sat} \sim 1$ A.

The temporal traces of bias current and voltage, line-average density, $\bar{n}$, H_α emission, measured by a photodiode looking tangentially to the plasma into the main limiter, ratio $\bar{n}/H_\alpha$, radiated power, P_{rad}, and floating potential and radial electric field, measured by the rake probe, are shown for a discharge with electrode bias (shot #11300) and without it (shot #11296), in the time interval of interest (the whole discharge lasts for approximately 40 ms). We note that the density increases and the H_α emission decreases during the polarization pulses, so that the ratio $\bar{n}/H_\alpha$ (which is roughly proportional to the particle confinement time τ_p) increases substantially. At the same time, the radiated power P_{rad} does not increase appreciably, so that the density rise can be unequivocally attributed to better particle confinement, as opposed to increased ionization by impurity penetration. The floating potential drops by almost 40 V with respect to the non-bias case, confirming that both the plasma potential and the edge radial electric field can be modified for negative applied voltages as previously observed on the limiter biasing experiments carried out in ISTTOK [21].

The particle confinement time was estimated, from density decay experiments, to be of the order of 0.5 ms in standard

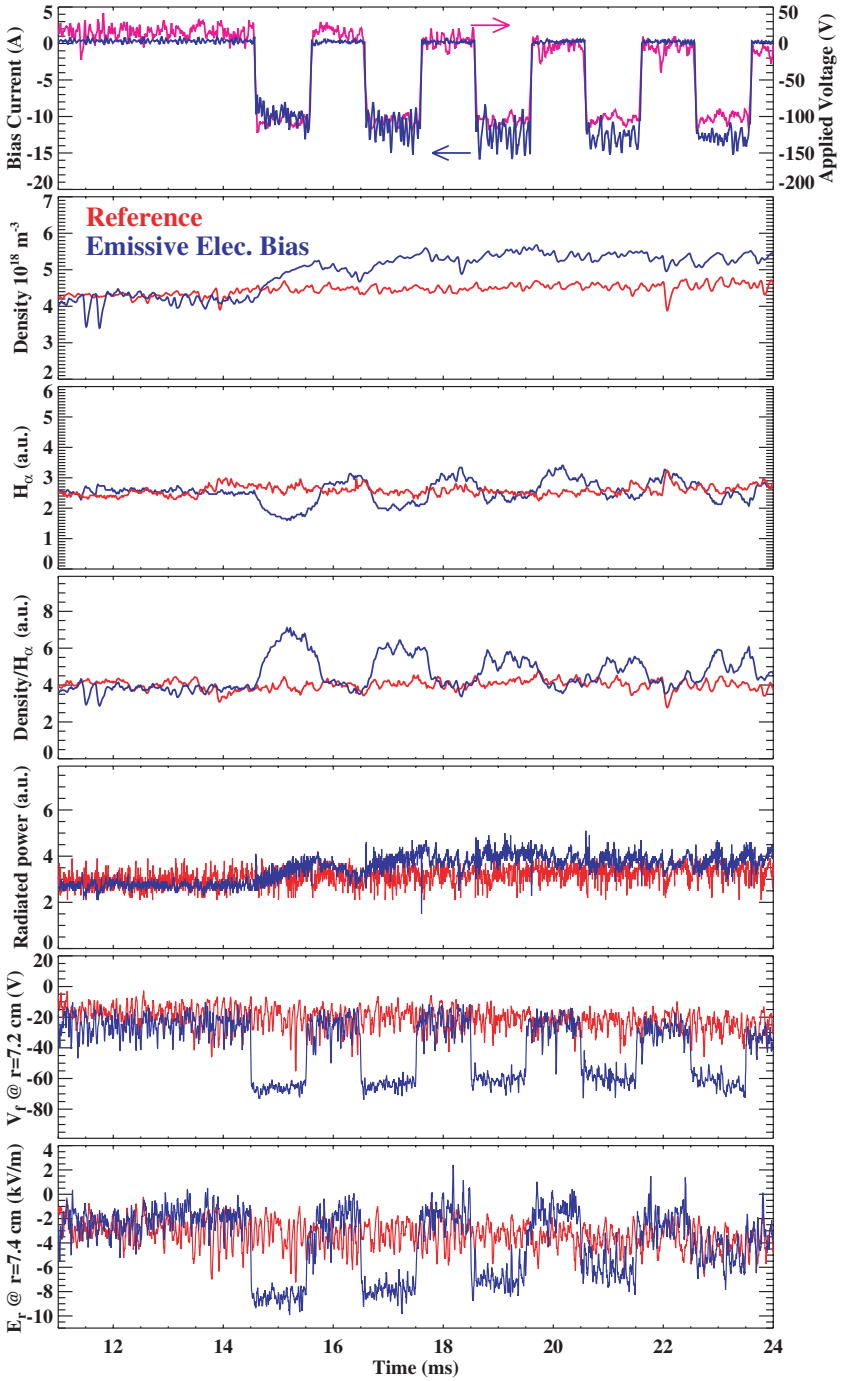

Figure 3. Time evolution of the main plasma parameters for a discharge with negative emissive electrode bias (shot #11300, $V_{\text{bias}} = -100$ V). The bias was applied in periodic pulses of 1 ms duration, with the same time interval between pulses. A discharge with no applied voltage is also shown for comparison.

ISTTOK discharges. Analysing in detail the density increase during the first polarization pulse, we obtain that indeed the density rises with a characteristic time $\tau_{\text{char}} \approx 0.5$ ms. However, after the polarization pulse, the density falls off with a somewhat larger characteristic time, so that a steady density build-up is observed between the pulses. A steady state at a larger density value is obtained after the third pulse, so that no more density increase is observed in subsequent pulses. This is possible related with the decrease of the modification in the radial electric for the later pulses.

3.1.1. Bias at large emission current. The time evolution of the main plasma parameters for a discharge with negative emissive electrode bias, $V_{\text{bias}} = -200$ V, and large bias current, $I_{\text{max}} \approx -25$ A, is presented in figure 4. The bias voltage is applied at $t \approx 16$ ms and the electrode is located 12 mm inside LCFS. As the bias is applied, the floating potential at the plasma edge is modified in a rather short time scale ($<50\,\mu$s), the bias current amplitude increases rapidly to a maximum value, around 20 A, and it starts to present a sawtooth behaviour, which will be discussed in detail in the following sections.

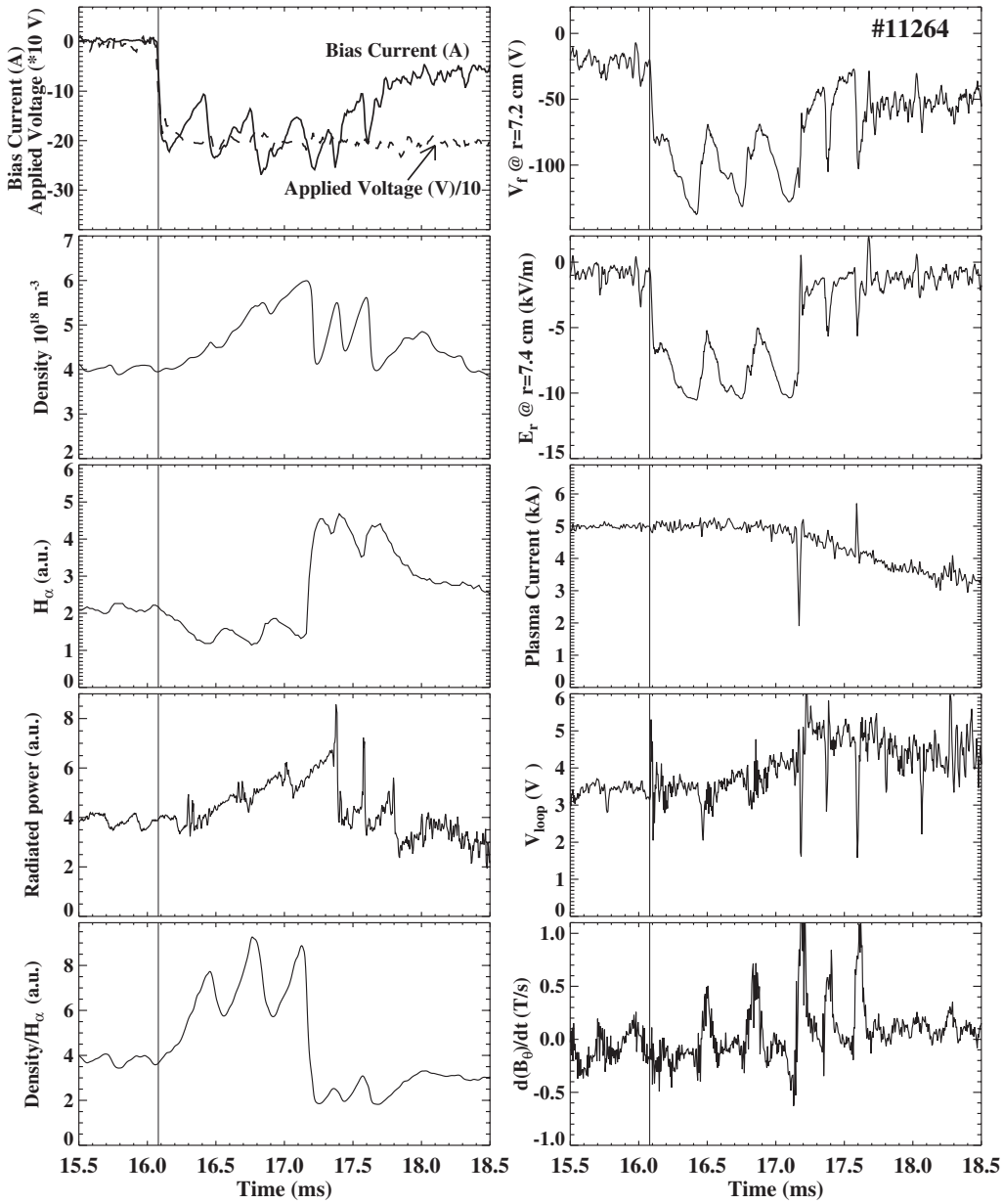

Figure 4. Time evolution of the main plasma parameters for a discharge with negative emissive electrode bias (shot #11264, $V_{\text{bias}} = -200$ V). The bias voltage is applied at $t \approx 16$ ms for 4 ms.

The rapid decrease of the floating potential occurs at the edge of the whole plasma column, as verified by probes separated approximately 120° in the toroidal direction. The floating potential decreases by about 60 V, at $r - a = -6$ mm, while close to the limiter it does not change significantly, leading to a strong modification in the edge radial electric field (from -1 to -7 kV m^{-1}) in the region just inside the limiter. The evolution of the radial profile of the electric field, during the sawtooth oscillations, will be discussed in the next section.

In spite of the oscillations observed in the emission current, the line-averaged density increases substantially, $\Delta\bar{n}/\bar{n} \approx 50\%$. In contrast to the low emission current case, the radiation losses also increase after the bias is applied. However, the rise remains roughly proportional to that observed in the density, so that there is no evidence for significant impurity influx during the bias. Furthermore, since the H_α radiation intensity decreases significantly, $\Delta I_{H_\alpha}/I_{H_\alpha} \approx -40\%$, after the bias is applied, there is clear indication of a reduction in recycling. The gross global particle confinement time, τ_p, almost doubles at the peak of the oscillations, as inferred from the ratio $\bar{n}/H_\alpha$.

The end of the improved confinement period ($t \approx 17.5$ ms) is probably a consequence of a MHD instability as fast perturbations in the plasma current, V_{loop} and Mirnov coils signals are observed at that time. In contrast, the modification on V_{loop} and Mirnov coils signals during the periodic degradations in confinement probably result from a modification in the plasma transport properties. It is worth noting that the parallel current collected by the electrode modifies significantly the edge current profile and may have detrimental effects on the MHD stability. Electrons are emitted in the direction opposite to the plasma current resulting therefore in a positive perturbation of

the edge current. As shown by Kesner *et al* [27], a positive current at the plasma edge has a destabilizing effect on modes with high m (m is the poloidal mode number), whereas a negative edge current is expected to improve plasma MHD stability.

3.1.2. Improved confinement events. We dubbed the periodic improvement on particle confinement as ICEs. They require a minimum bias current and are characterized by (see figure 4): (i) a further increase in the magnitude of the radial electric field (or a modification of its profile); (ii) a reduction in the amplitude of the collected current (although the bias voltage remains constant) and (iii) a strong increase in particle confinement. The latter reaches its maximum during ICEs, clearly exceeding the particle confinement observed in discharges without these events (see figure 3). Provided that the amplitude of the bias current is larger than the threshold value, ICEs may be observed at any time during the biased period and lasting typically less than 400 μs. As will be discussed later, these events may be associated with a bifurcation in the radial electric field [17].

The good confinement properties of the plasma are periodically lost in a short time scale ($<$50 μs). This degradation in confinement is characterized by a: (i) reduction in density and radiation losses; (ii) rise in H_α radiation intensity; (iii) fast increase of the collected current amplitude, associated with reduction of the edge radial electric field and (iv) sharp increase of both the turbulent particle flux and the density near the limiter. In most of the discharges, we observe no more than two or three consecutive cycles of ICEs.

It is interesting to note that very similar events were observed in the emissive edge biasing experiments carried out in the MST reversed field pinch [23]. In their case, the bias current was much larger than in ISTTOK experiments, approximately 3 kA, and the events have been attributed to sawtooth oscillations associated to reconnection events of the toroidal magnetic field at the wall [28]. The situation is quite the opposite in ISTTOK, as the maximum value of $I_{\rm bias}$ is around 30 A and no distinctive sawtooth-like MHD activity is observed during the events. In spite of these differences, other signatures of the ICEs are quite similar. In particular, the radial electric conductivity of the plasma, $I_{\rm bias}/E_r$, is observed to decrease substantially, upon entering the enhanced confinement regime, as in electrode biasing experiments in other tokamaks [1–4], and the relative increase of the particle confinement time is approximately equal in both devices.

Figure 5 shows the time evolution of the floating potential, ion saturation current, and the cross-field turbulent flux, $\Gamma_{E\times B} = \langle \tilde{n}\tilde{E}_\theta \rangle / B$, where E_θ is the poloidal electric field and B is the toroidal magnetic field, during a discharge with EEB. The bias was applied at $t = 20.6$ ms for 1 ms. The average turbulent transport is reduced after the bias is applied, decreasing periodically during each ICE. These periods of reduced transport are separated by bursts associated with the increase of the bias current. Both the $I_{\rm sat}$ and $V_{\rm f}$ fluctuation levels are reduced by a factor of approximately 2 when negative EEB is applied. A further reduction in the $I_{\rm sat}$ fluctuation level (up to a factor of 10 over its value before bias) is observed during ICEs. Therefore, the observations are consistent with a local reduction of the anomalous particle flux, as a result of a reduced electrostatic turbulence.

3.1.3. Evolution of the radial plasma profiles. To better characterize the modifications introduced by the electrostatic polarization at the plasma edge, we have measured the evolution of the radial electric field profile. The time evolution of the bias current, ratio $\tilde{n}/H_\alpha$ and radial profile of the floating potential is shown in figure 6(a). The radial profiles of $V_{\rm f}$ and E_r at relevant times (indicated in figure 6(a)) are shown in figure 6(b) following the same colour scheme. The plasma potential is derived from $V_{\rm p} = V_{\rm f} + 3T_{\rm e}$. For most of the discharges, no temperature measurements with high temporal resolution are available. However, since it was found that the edge temperature does not change significantly during biasing, the average $T_{\rm e}$ profile is used in the evaluation of $V_{\rm p}$. Furthermore, during bias the radial electric field is not strongly affected by temperature uncertainties because the contribution of the $V_{\rm f}$ gradient is much larger than that of the temperature gradient. This is illustrated by the error bars in figure 6(b), which for the floating potential represent the standard deviation of $V_{\rm f}$, whereas for the radial electric field represent the effect of a 5% temperature error in the E_r estimation.

As the bias is applied, a large electric field with a double-peaked structure is observed. Afterwards, the profile slowly evolves to a single-peaked profile as the collected current amplitude decreases, reaching a value of $-12\,{\rm kV\,m^{-1}}$ in the region just inside the limiter, associated with a strong E_r shear ($\mathrm{d}v_{E\times B}/\mathrm{d}r \approx 3\times10^6\,{\rm s^{-1}}$ at $r-a=0$ mm). The velocity shear rate ($\mathrm{d}v_{E\times B}/\mathrm{d}r$) exceeds significantly the inverse of the correlation time of fluctuations, $1/\tau \approx (1\text{–}2)\times10^5\,{\rm s^{-1}}$. Therefore, the amplitude of the velocity shear rate is of the proper magnitude to suppress the turbulent fluctuations in the ISTTOK edge plasma. This is corroborated by probe measurements, which show a decrease of the turbulent particle transport when the bias is applied (see figure 5).

The data presented correspond to a representative EEB discharge; however, the effect of bias has small variations from discharge to discharge, depending on plasma conditions. In general, the modifications in the radial electric field E_r during EEB, with $V_{\rm bias} < -125$ V, can be summarized as follows: (i) fast increase ($<$50 μs) in E_r just inside the limiter radius, following the fast increase in the bias current; (ii) during the ICEs, E_r slowly increases as the collected current amplitude slowly decreases; (iii) double-peaked E_r profiles are often observed just after biasing; (iv) when a double-peaked structure appears, the E_r profile evolves during the events to a single peak, without a significant increase in the maximum magnitude of E_r; (v) the improved confinement is periodically destroyed and the floating potential profile returns to a profile very similar to that just after the bias and (vi) the end of the improved confinement period is characterized by a large reduction of E_r inside the region $r-a < -4$ mm. For moderate bias voltages ($-125 < V_{\rm bias} < -75$ V), the collected current and the radial electric field are in general too low to drive ICEs. Under this condition, only a moderate improvement in particle confinement is obtained, $\Delta\tau_{\rm p}/\tau_{\rm p} \approx 40\%$, and no double-peaked profiles are observed.

The evolution of the edge ion saturation current radial profiles during biasing, measured with the rake probe, is illustrated in figure 7. The $I_{\rm sat}$ signal may be assumed to be mainly proportional to the density, since it has a week dependence on the temperature ($I_{\rm sat} \propto nT_{\rm e}^{1/2}$) and the latter

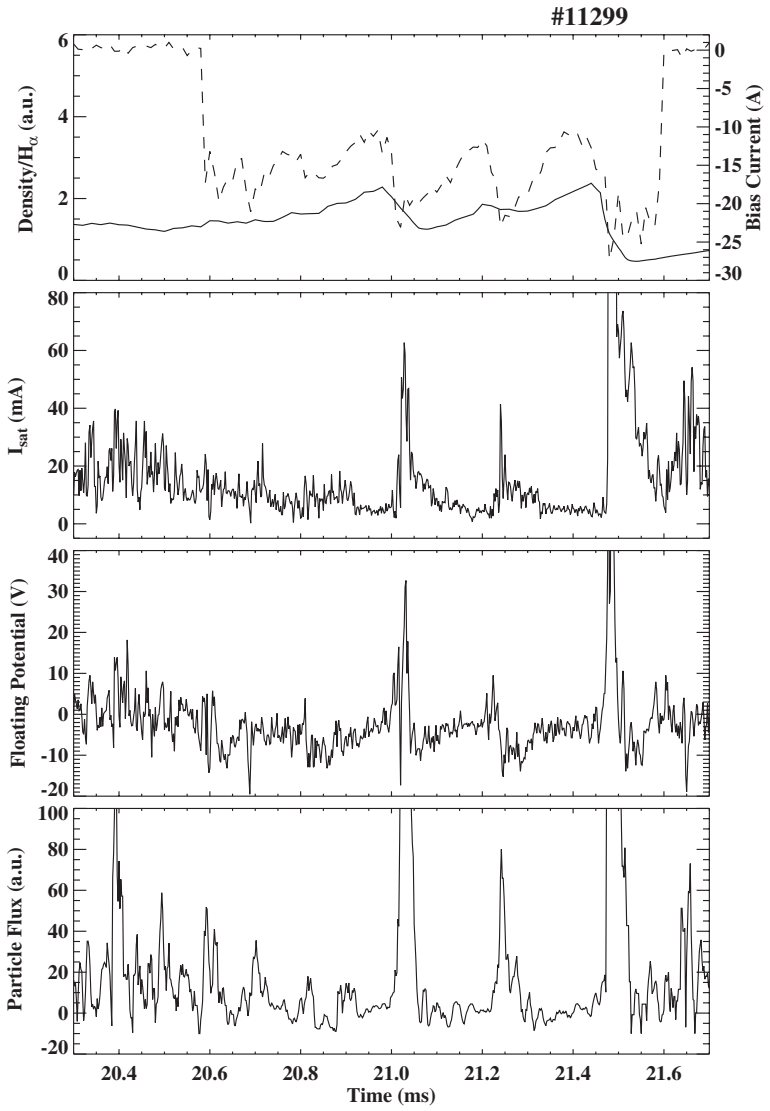

Figure 5. Time evolution of the collected current and particle confinement together with the ion saturation current, floating potential and turbulent particle flux at $r = a$ for a discharge with emissive electrode bias. The bias voltage (-175 V) is applied at $t = 20.6$ ms for 2 ms.

does not vary significantly during biasing. For negative bias, $I_{\rm sat}$ measurements are not valid in the region $r-a < -5$ mm as the applied voltage, -150 V, is not enough to drive the probes into saturation (the floating potential reaches very negative values in this region, figure 6(*b*)). As a consequence, for negative bias, profiles are only shown in the region $r - a > -5$ mm. The results show clearly that the edge density profile becomes stepper as the bias is applied. Furthermore, during ICEs the edge density gradient increases even more, with a clear density reduction observed across most of the scrape-off layer. These results are consistent with the observed reduction on the fluctuation induced particle flux (figure 5) and suggest that confinement enhancement originates at the edge plasma as a consequence of the formation of a particle transport barrier near the limiter.

The ISTTOK HIBD has also been used to characterize discharges with emissive electrode bias. We observed that the $n_{\rm e}\sigma_{\rm eff}$ time evolution during bias is well correlated with that of the line-averaged density. Furthermore, during biasing $n_{\rm e}\sigma_{\rm eff}$ is observed to increase across the whole profile, being that increase larger for negative bias. This is illustrated in figure 8, which shows the radial profiles of $n_{\rm e}\sigma_{\rm eff}$ measured by the different detector cells for positive and negative bias voltages. Because the temperature does not change significantly in a short time scale (1 ms) after biasing, the modifications in the $n_{\rm e}\sigma_{\rm eff}$ profile can be attributed mainly to a change in the density profile. We have observed with the Langmuir probe array that the density near the limiter decreases for negative bias (see figure 7), leading therefore to a strong increase in the edge density gradient.

3.2. Positive electrode bias

For large positive bias ($V_{\rm bias} > 50$ V), the emissive current is zero and therefore there is no significant difference between hot and cold electrode bias. Figure 9 shows the time evolution of the main plasma parameters of a discharge with positive electrode bias (+140 V). As can be seen from the floating

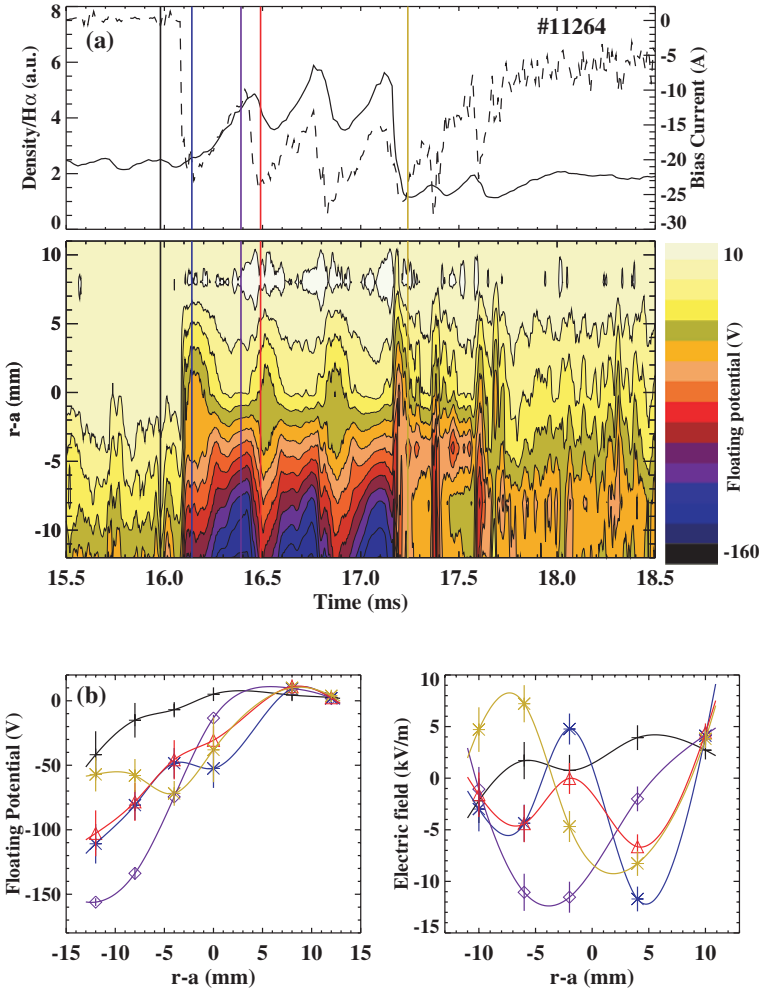

Figure 6. (*a*) Time evolution of the collected current, ratio $\bar{n}/H_\alpha$ and floating potential radial profiles for the discharge #11264. (*b*) Radial profiles of the floating potential and radial electric field for the times indicated in (*a*).

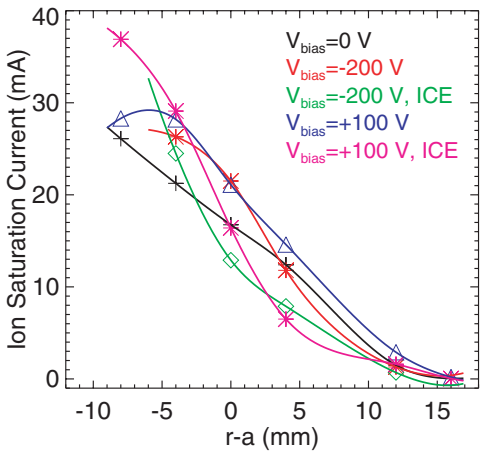

Figure 7. Evolution of the I_{sat} radial profiles during negative and positive bias.

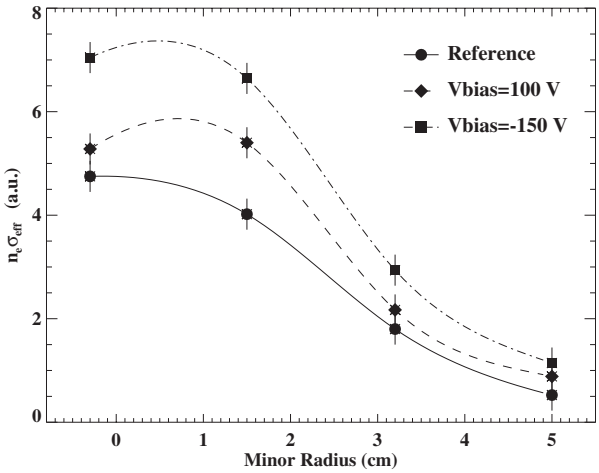

Figure 8. Radial profiles of $n_e\sigma_{eff}$ for positive (- - - -) and negative (— · —) bias voltages. The radial profile without bias is also shown for comparison (——).

potential variation, the radial electric field profile is modified, leading to a plasma density increase in this case too. However, contrary to the results obtained for negative EEB, the H_α radiation also increases during biasing, causing a rather modest increase in particle confinement. Furthermore, as observed in previous experiments carried out in ISTTOK [3], the positive bias tends to increase recycling. The larger recycling for positive may result from the substantial ion return current driven to the wall (>20 A).

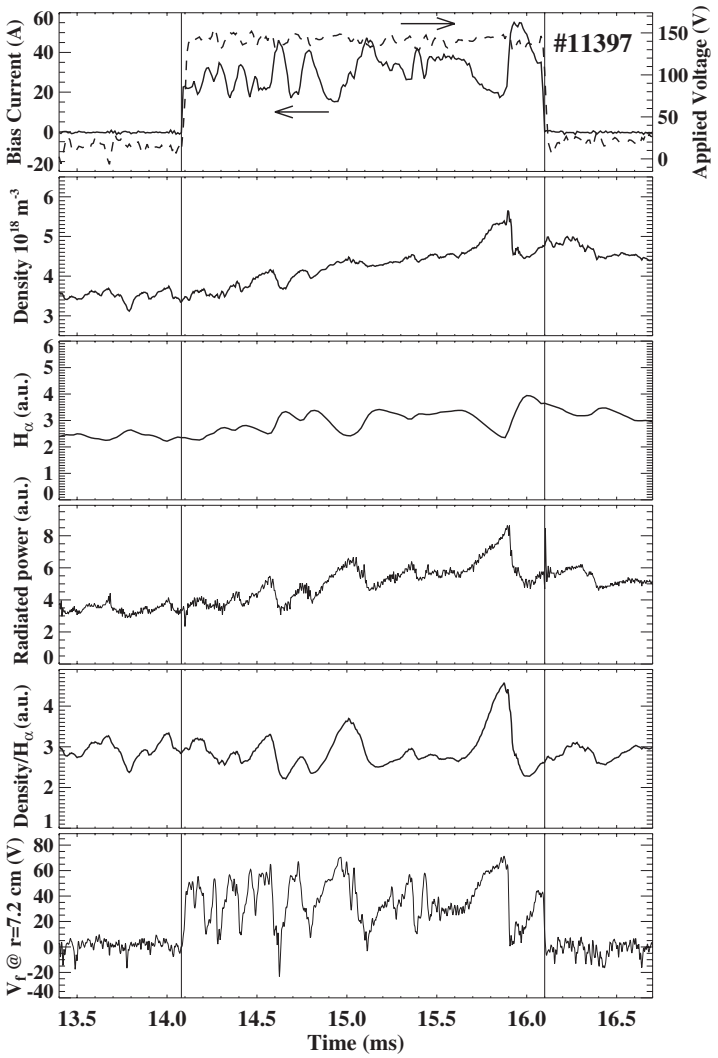

Figure 9. Time evolution of the main plasma parameters for a discharge with positive emissive electrode bias (shot #11397, $V_{\text{bias}} = 140$ V). The bias voltage was applied at $t = 14.1$ ms for 2 ms.

The ICEs occur also for positive electrode bias, with characteristics similar to the events at negative EEB. Again a minimum current of $I_{\text{bias}} \approx 20$ A seems to be required to trigger them. During the ICEs, the radial electric field increases, in spite of the reduction in the collected current, and the particle confinement increases transiently, for very short periods between 0.3 and 0.5 ms. However, the ICE's duration, frequency and amplitude are in general less regular for positive bias when compared with negative one.

The time evolution of the bias current, ratio $\bar{n}/\mathrm{H}_\alpha$, and radial profile of the floating potential is shown in figure 10(*a*), for the same discharge of figure 9. The radial profile of V_{f} and E_r, at relevant times indicated in figure 10(*a*), are shown in figure 10(*b*) following the same colour scheme. The edge E_r reaches a maximum when the current attains its minimum. The radial electric field is only significant (>5 kV m^{-1}) within a narrow region (<8 mm) around the limiter radius, whereas for negative bias the region of enhanced field starts just inside limiter radius and extends for more than 10 mm. It is interesting to note that for positive bias no double-peaked structures are observed in the radial electric field, suggesting that these structures are related with transitory localized space charge formation, caused by the emitted electrons.

The evolution of the edge I_{sat} and $n_{\text{e}}\sigma_{\text{eff}}$ profiles for positive electrode bias is also presented in figures 7 and 8, respectively. The edge density is observed to increase in the region $r - a > -10$ mm when the bias is applied (figure 7), which is in agreement with the observed increase in recycling. However, during the transient increase in particle confinement, steep edge density gradients are observed. Concerning the HIBD data (figure 8), it is observed that the density gradient is smaller for positive bias when compared to that at negatives bias as the density at the limiter increases slightly during biasing and the density rise measured by the HIBD at $r \approx 5$ cm is smaller than that observed for negative bias.

3.3. Perpendicular conductivity

The relation between the radial current density, $j_r = I_{\text{bias}}/4\pi^2 Ra$, and the radial electric field E_r was determined during the ICEs for a discharge with negative (#11386, -200 V) and another with positive (#11397, +140 V) applied voltage. The results are shown in figure 11. The radial electric

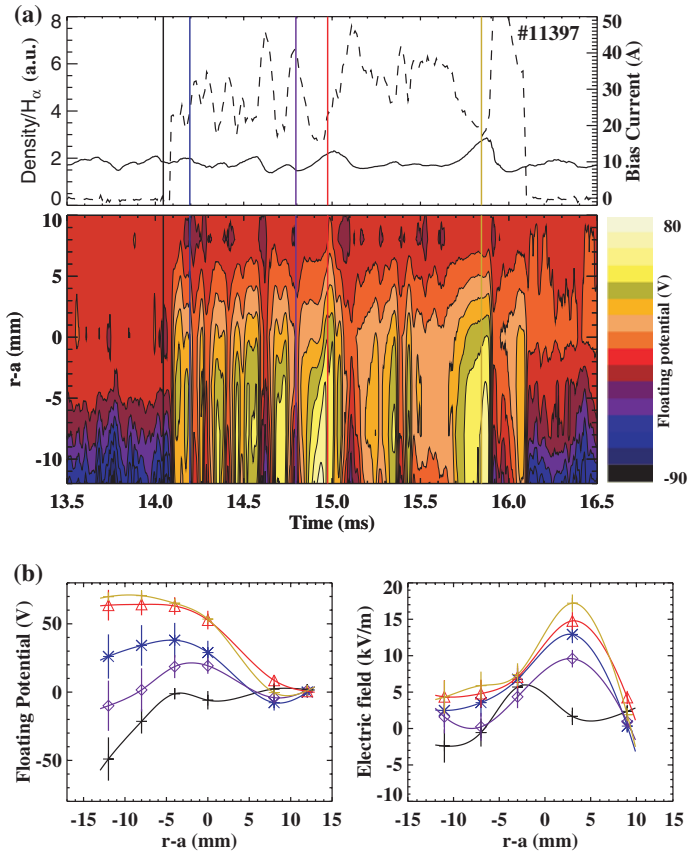

Figure 10. (*a*) Time evolution of the collected current, ratio $\bar{n}/H_\alpha$ and floating potential radial profiles for the discharge #11397. (*b*) Radial profiles of the floating potential and radial electric field for the times indicated in (*a*).

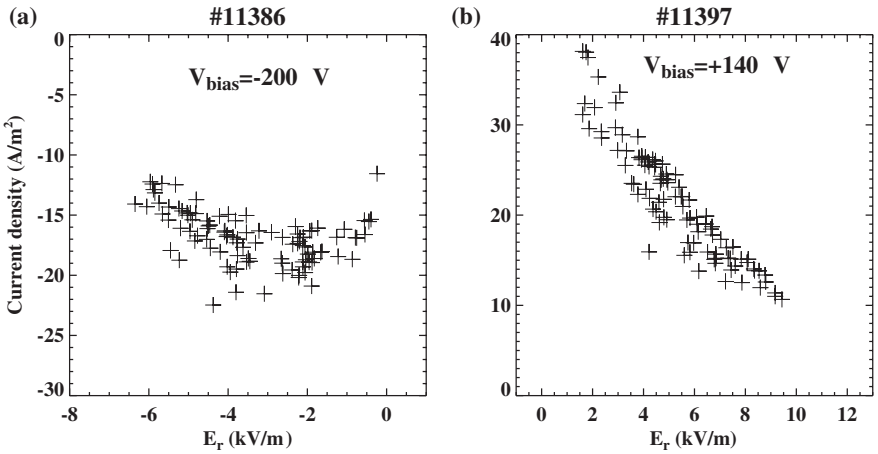

Figure 11. Variation of the bias current density with the radial electric field for a discharge with negative (*a*) and positive (*b*) EEB.

field was calculated using the floating potential measured by two probes radially separated by 12 mm, being the outermost probe located just outside the limiter radius. As shown earlier, the ICEs are observed for both polarities, above a certain current threshold. During these events, the amplitude of the collected current decreases as the particle confinement and E_r augment, resulting in the inversed dependence of j_r on E_r for large values of the polarization voltage, as originally pointed out by Weynants and Taylor [2]. In the case of ISTTOK, the value of the conductivity at the maximum of the radial current is $\sigma \approx 3.5 \times 10^{-3}\ \Omega^{-1}\ m^{-1}$. After the saturation of the radial current density, the perpendicular conductivity decreases sharply with the radial electric field [2–4], in qualitative agreement with the Stringer model, as will be discussed in the next section.

4. Discussions and conclusions

The reduction of the plasma conductivity as the plasma enters the enhanced confinement regime confirms the results obtained

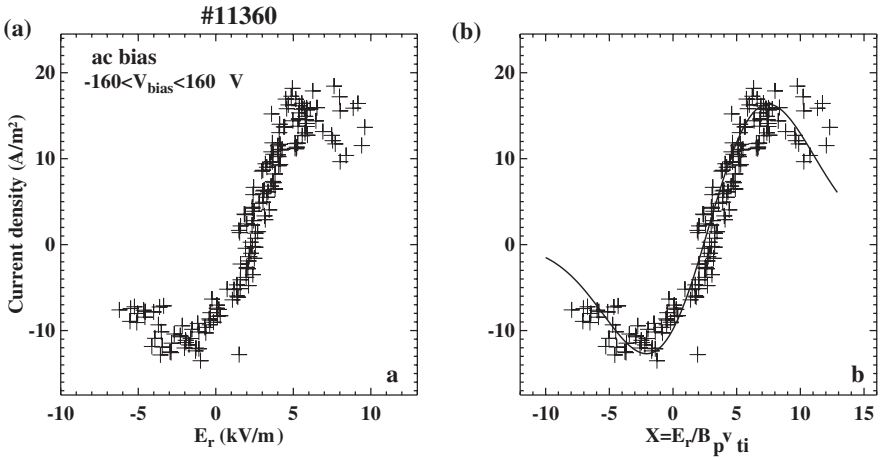

Figure 12. Variation of the bias current density with the radial electric field (a) and with the normalized parameter $x = E_r/v_{\rm ti}B_{\rm p}$ (b) for a discharge with ac EEB. The solid line shows the fit of the experimental data to equation (1).

in other tokamaks [1, 2, 22] and seems to be in qualitative agreement with the neoclassical theories for the damping of poloidal rotation [29] and for the radial current density [17]. To check the latter point in more detail, we have carried out EEB experiments with alternating bias voltage (50 Hz, 160 V peak voltage). Since the maximum duration of the discharges was around 50 ms, we obtained at most two complete polarization cycles per discharge and they were not phase-locked with the discharge initiation. Therefore, the ac polarization could not be applied for reproducible plasma conditions, in particular regarding the plasma density. Nevertheless, we were able to obtain a sufficient number of discharges with approximately similar values of the relevant plasma parameters. The evolution of the radial current density with E_r is shown in figure 12(a), for one of the discharges with ac EEB. It is clear that the magnitude of the current increases roughly linearly with E_r up to a threshold value, where a bifurcation is observed [2, 17]. Above that value, the amplitude of the current decreases with increasing E_r, as observed during the ICEs.

According to Stringer, the radial current density can be expressed in terms of the imaginary part of the plasma dispersion function, $Z(\zeta)$, where $\varsigma = x + {\rm i}y$, $x = E_r/v_{\rm ti}B_{\rm p}$ is the normalized radial electric field, and $y = r\nu_{\rm ii}B/v_{\rm ti}B_{\rm p}$ is the ratio of the connection length to mean free path. In these expressions, $v_{\rm ti}$ is the thermal speed of the ions, r is the radial coordinate, $\nu_{\rm ii}$ is the ion–ion collision frequency and B and $B_{\rm p}$ are the toroidal and poloidal components of the magnetic field, respectively. From this dependence, it follows that the current first increases with the applied electric field and then decreases, owing to either the resonant velocity band being pushed to the tail of the ion velocity distribution or a decrease in the viscous damping. The current density has a zero field offset due to the ambipolar electric field $E_{\rm a}$, which is expressed in terms of the normalized constant $x_{\rm a}$ [17]. For the conditions of the EEB discharges in ISTTOK, the estimated value of the collisionality parameter is $y \approx 0.1$, so that plasma conditions are somewhat between the plateau and the collisional regimes. In this case, the imaginary part of the plasma dispersion function goes like $\exp(-x^2)$, to lowest order. Considering that the measurements of the radial electric field may have an offset not entirely compensated by our estimation of the ambipolar electric field ($E_{\rm a} \approx 0.5$–$1.5\,{\rm kV\,m^{-1}}$) and that the normalized quantity x may have a large uncertainty due to lack of measurement of the ion temperature and its variation during polarization, we have tried to fit the results with the expression

$$j_r \approx j_0(x - x_{\rm a})\,{\rm e}^{-\sigma(x-x_{\rm b})^2}, \qquad (1)$$

where j_0, $x_{\rm a}$, $x_{\rm b}$ and σ are fitting parameters, as an approximation to the correct expression of Stringer. The results of figure 12(a) are plotted again, in terms of the normalized quantities, in figure 12(b). The full curve corresponds to a fitting with $j_0 = 6\,{\rm A\,m^{-2}}$, $x_{\rm a} = 2.4$, $x_{\rm b} = 3.0$ and $\sigma = 0.025$. One interesting point to note is that the zero field offset of curve is displaced to a positive value of x, whereas, according to the neoclassical expression, it should be displaced to a negative value. One possible explanation for this feature is enhanced ion losses caused by ripple or error field losses, which can be important in small tokamaks [30] (this effect will be better investigated in controlled ripple experiments to be soon carried out in ISTTOK). Nevertheless, following Stringer, if we take $j_0 = \sqrt{\pi}(a/R)^2 n k_{\rm B} T_{\rm i}/(rB)$, where n and $T_{\rm i}$ are the ion density and temperature, respectively, we obtain $T_{\rm i} \approx 25\,{\rm eV}$, for the experimental value of the edge density, $n \approx 1.0 \times 10^{18}\,{\rm m^{-3}}$. This value is rather close to the value of the edge electron temperature measured in these discharges, confirming the estimated value for the collisionality parameter y. Furthermore, from this result and the value for $x_{\rm a}$, we obtain $E_{\rm a} \approx 1.5\,{\rm kV}$, in reasonable agreement with estimates based upon the measured profile of electron temperature taking also into account that the experimentally determined $E_{\rm a}$ has small variations depending on the region where it is measured.

Another point that deserves further close study is the variation of the radial electric field profiles during the ICEs, for negative polarization (shown in figure 6(b)). As previously mentioned, the profile presents a double-peaked structure right after the application of the bias voltage, indicating that a negative space charge is formed in a radial position close to the electrode. This charge perturbation dissipates away as the density increases during the event. The transient double-peaked profile may be related to the non-linear structures

discussed by Kasuya *et al* [18, 19]. In their case, the non-linear structures have two double peaks with the same polarity, whereas we observe them with inverted polarities. This occurs because they have integrated the non-linear equation for the normalized radial electric variable x imposing only the initial condition $\mathrm{d}x/\mathrm{d}r = 0$, which imposes symmetric solutions. However, as pointed out by Stringer, the correct constraint on the non-linear solutions is $\int E_r \, \mathrm{d}r = V_{\mathrm{bias}}$, where the integral is to be carried out between the emissive electrode and the grounded vacuum chamber. In this case, non-linear solutions associated with localized space charges have to show inversion of the electric field at the charge localization [17]. However, it is interesting to note that in spite of the larger shear observed when two peaks of E_r are present, the improvement in confinement is modest during these periods (∼20–30%), only increasing significantly when V_{f} evolves to a monotonic profile (see figure 6).

Although the neoclassical theory seems to explain the reduction in σ_{r} during ICEs, it cannot explain the fast relaxation of the poloidal rotation after the bias is switched off. The decay time of the collected current is roughly 10 μs, as the bias voltage is switched off and the characteristic time of the radial electric field drop is around ∼20 μs. The evolution of plasma flows after the application of an external biasing has been previously investigated and the damping times found are in the range of 10–30 μs [31, 32]. This time is much smaller than the expected damping time based on magnetic pumping mechanism (∼100 μs) and atomic physics via charge exchange (∼500 μs) and only slightly larger than the correlation time of plasma turbulence (10 μs), indicating that anomalous viscosity may play and important role in edge poloidal damping.

In summary, the first experimental results of edge polarization experiments with emissive electrodes, carried out in ISTTOK, have been presented. We have shown that the edge plasma potential can be modified for both polarities in opposition to that observed with non-emissive electrodes. Furthermore, an improvement on particle confinement is clearly observed for negative EEB. Above a certain threshold of the bias current improved confinement events are observed for both bias polarities, which are characterized by a further improvement in confinement during short periods.

Acknowledgments

This work has been carried out within the framework of the Contract of Association between the European Atomic Energy Community and 'Instituto Superior Técnico'. Financial support was also received from 'Fundação para a Ciência e Tecnologia' and 'Programa Operacional Ciência, Tecnologia, Inovação do Quadro Comunitário de Apoio III'. One of us (RMOG) would also like to acknowledge partial support from National Council for Scientific and Technological Development and The State of São Paulo Research Foundation (Brazil).

References

[1] Taylor R.J., Brown M., Fried B.D., Grote H., Liberati J.R., Morales G.J., Pribyl P., Darrow D. and Ono M. 1989 *Phys. Rev. Lett.* **63** 2365
[2] Weynants R.R. and Taylor R.J. 1990 *Nucl. Fusion* **30** 945
[3] Shimada M., Ozaki A., Petersen P., Riedy P., Petrie T., Janeschitz G. and Mahdavi M. 1990 *J. Nucl. Mater.* **176–177** 821
[4] Weynants R.R. *et al* 1992 *Nucl. Fusion* **32** 837
[5] Doerner R.P., Boedo J.A., Conn R.W., Gray D.S., Tynan G.R., Baek W.Y., Dippel K.H., Finken K.H. and Moyer R.A. 1994 *Nucl. Fusion* **34** 975
[6] Cabral J.A.C. *et al* 1998 *Plasma Phys. Control. Fusion* **40** 1001
[7] Stöckel J. *et al* 1999 *Plasma Phys. Control. Fusion* **41** A577
[8] van Oost G. *et al* 2003 *Plasma Phys. Control. Fusion* **45** 621
[9] Cornelis J.E., Sporken R., van Oost G. and Weynants R.R. 1994 *Nucl. Fusion* **34** 171
[10] Askinazi L.G., Golant V.E., Lebedev S.V., Rozhanskij V.A. and Tendler M. 1992 *Nucl. Fusion* **32** 271
[11] Rozhanskij V. and Tendler M. 1996 *Reviews of Plasma Physics* vol 19 (New York: Consultants Bureau)
[12] Heikkinen J.A., Jachmich S., Kiviniemi T.P., Kurki-Suonio T. and Peeters A.G. 2001 *Phys. Plasmas* **8** 2824
[13] Ida K. 1998 *Plasma Phys. Control. Fusion* **40** 1429
[14] Stacey W.M. 1993 *Phys. Fluids* B **5** 1413
[15] Rogister A.L. 1994 *Plasma Phys. Control. Fusion* **36** A213
[16] Itoh K., Itoh S.-I., Yagi M. and Fukuyama A. 1998 *Phys. Plasmas* **5** 4121
[17] Stringer T.E. 1993 *Nucl. Fusion* **33** 1249
[18] Kasuya N., Itoh K. and Takase Y. 2003 *Nucl. Fusion* **43** 244
[19] Kasuya N., Itoh K. and Takase Y. 2003 *J. Plasma Fusion Res.* **79** 543
[20] Silva C., Figueiredo H., Nedzelskiy I., Gonçalves B, Cabral J.A.C., Varandas C.A.F. and van Oost G. 2004 *Plasma Phys. Control. Fusion* **46** 173
[21] Silva C., Nedzelskiy I., Figueiredo H., Cabral J.A.C., Varandas C.A.F. and Stöckel J 2003 *Czech. J. Phys.* **53** 937
[22] Taylor R.J. and Oren L. 1979 *Phys. Rev. Lett.* **42** 446
[23] Craig D. *et al* 1997 *Phys. Rev. Lett.* **79** 1865
[24] Schrittwieser R., Adámek J., Balan P., Hron M., Ionita C., Kryska L., Martines E., Stöckel J., Tichy M. and van Oost G. 2002 *Plasma Phys. Control. Fusion* **44** 567
[25] Ye M.Y. and Takamura S. 2000 *Phys. Plasmas* **7** 3457
[26] Ishiguro S. and Sato N. 1993 *Phys. Fluids* B **5** 4237
[27] Kesner J., Ramos J.J. and Luckhardt S.C. 1994 *Nucl. Fusion* **34** 795
[28] Prager S.C. *et al* 1990 *Phys. Fluids* B **2** 1367
[29] Chaing K.C. and Crume E.C. 1989 *Phys. Rev. Lett.* **63** 2369
[30] Dallaqua R. *et al* 1984 *Il Nuovo Cimento* B **83** 1
[31] Hron M., Hidalgo C., Pedrosa M.A., Duran I. and Stöckel J. 2003 On the relaxation physics of the plasma potential and poloidal flows in plasma: experiments in tokamak (Castor) and stellarator (TJ-II) *14th International Stellarator Workshop (22–26 September, 2003)*
[32] Hidalgo C. *et al* 2004 *Plasma Phys. Control. Fusion* **46** 287